Structural and biochemical insights into the dicing mechanism of mouse Dicer: A conserved lysine is critical for dsRNA cleavage

Zhihua Du[†], John K. Lee[‡], Richard Tjhen[†‡], Robert M. Stroud[†‡§], and Thomas L. James[†§]

Departments of [†]Pharmaceutical Chemistry and [‡]Biochemistry and Biophysics, University of California, San Francisco, CA 94158-2517

Contributed by Robert M. Stroud, December 17, 2007 (sent for review November 16, 2007)

Dicer, an RNase III enzyme, initiates RNA interference by processing precursor dsRNAs into mature microRNAs and small-interfering RNAs. It is also involved in loading and activation of the RNA-induced silencing complex. Here, we report the crystal structures of a catalytically active fragment of mouse Dicer, containing the RNase IIIb and dsRNA binding domains, in its apo and Cd^{2+}-bound forms, at 1.68- and 2.8-Å resolution, respectively. Models of this structure with dsRNA reveal that a lysine residue, highly conserved in Dicer RNase IIIa and IIIb domains and in Drosha RNase IIIb domains, has the potential to participate in the phosphodiester bond cleavage reaction by stabilizing the transition state and leaving group of the scissile bond. Mutational and enzymatic assays confirm the importance of this lysine in dsRNA cleavage, suggesting that this lysine represents a conserved catalytic residue of Dicers. The structures also reveals a ≈45-aa region within the RNase IIIb domain that harbors an α-helix at the N-terminal half and a flexible loop at the C-terminal half, features not present in previously reported structures of homologous RNase III domains from either bacterial RNase III enzymes or *Giardia* Dicer. N-terminal residues of this α-helix have the potential to engage in minor groove interaction with dsRNA substrates.

dsRNA processing | RNA interference | RNase III | x-ray crystallography

The innate gene silencing mechanism of RNA interference (RNAi) is triggered by small dsRNAs (1, 2). Fundamental roles of RNAi include defense against viruses (3), regulation of development (4), and genome maintenance (5, 6). The two major classes of small RNAs responsible for this mechanism are microRNAs (miRNAs) and small-interfering RNAs (siRNAs) (7, 8); both are generated by the riboendonuclease Dicer (9, 10).

Dicer processes precursor miRNAs (pre-miRNA, generated by the riboendonuclease Drosha in the nucleus from the primary transcripts of miRNAs) and long dsRNAs (generated during viral infections or introduced experimentally into the cell) into mature miRNAs/siRNAs. It then loads the miRNA/siRNA into the Argonaute–containing RNAi effector complex RNA-induced silencing complex (RISC) (11). The passenger strand of the miRNA/siRNA is cleaved by Argonaute and discarded (12, 13); the guide strand leads RISC to target mRNAs with sequence motifs complementary to that of the guide. The result is either mRNA degradation or translational suppression (10, 14). Structures of Argonaute and related proteins have contributed to these insights into the mechanisms of Argonaute activities (for reviews see refs. 15 and 16 and references therein).

Dicer is an RNase III enzyme specific for dsRNAs. RNase III cleavage products contain 5′ phosphate and 3′ hydroxyl termini and a 2-nt overhang at the 3′ end. Dicer products are also characterized by its discrete size of ≈21 nt (17). RNase III enzymes can be divided into three classes (Fig. 1). Class I enzymes, found in bacteria, bacteriophage, and fungi, contain a single RNase III domain and a dsRNA binding domain (dsRBD). Class II and III are characterized by Drosha and Dicer, respectively. Dicer is the most complicated RNase III enzyme that typically contains a DExD/H-box helicase domain,

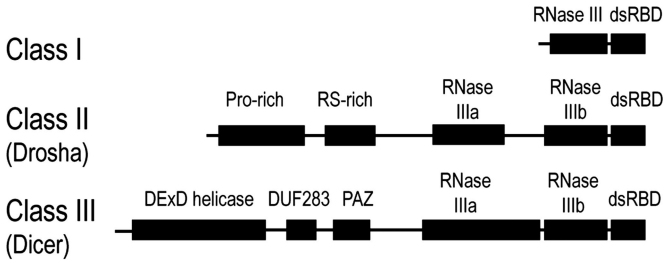

Fig. 1. A schematic representation of the three classes of RNase III enzymes. Protein domains are indicated as black rectangles.

a small domain of unknown function (DUF283), a PAZ (Piwi Argonaute Zwille) domain, two tandem RNase III domains (RNase IIIa and IIIb), and a dsRBD. Some Dicer or Dicer-like proteins from lower eukaryotes have a simpler domain structure; for example, the Dicer protein from *Giardia intestinalis* contains only a PAZ and two RNase III domains (18). Previous mutational and enzymatic studies on *Escherichia coli* RNase III and human Dicer had led to the "single processing center model" for RNase III cleavage (19). This model centers on two RNase III domains forming a catalytic dimer: intermolecular homodimer for class I enzymes and intramolecular pseudodimer between RNase IIIa and IIIb domains for Dicer and Drosha. This dimerization creates a single processing center for dsRNA cleavage, with each RNase III domain cleaving one strand of the dsRNA. The distance between the two cleavage sites dictates the generation of the characteristic 2-nt 3′ overhang. For Dicer, the distance between the terminus-binding PAZ domain and the RNase III domains determines the length of the cleavage product.

Two recent crystal structures have provided strong support of the single processing center model: *Aquifex aeolicus* RNase III enzyme bound to dsRNA cleavage products at 2.05-Å resolution (20) and *Giardia* Dicer at 3.33-Å resolution (18). The structure of the *Aquifex* RNase III–dsRNA complex reveals that four patches of residues, termed RNA-binding motifs 1–4 (RBM1–RBM4), are involved in protein–RNA interaction. RBM1 and RBM2 are located in the dsRBD, and RBM3 and RBM4 are located in the RNase III domain. A flexible linker of 7 aa between the RNase III and dsRBD domains allows induced

Author contributions: Z.D. designed research; Z.D. and J.K.L. performed research; Z.D., J.K.L., R.T., R.M.S., and T.L.J. analyzed data; and Z.D., J.K.L., R.M.S., and T.L.J. wrote the paper.

The authors declare no conflict of interest.

Data deposition: The atomic coordinates have been deposited in the Protein Data Bank, www.pdb.org (PDB ID codes 3C4B and 3C4T).

[§]To whom correspondence may be addressed. E-mail: stroud@msg.ucsf.edu or james@picasso.ucsf.edu.

This article contains supporting information online at www.pnas.org/cgi/content/full/0711506105/DC1.

fit of the relative orientation of the two domains upon binding dsRNA. At each of the two active sites, the four conserved catalytic carboxylates (two aspartates and two glutamates) and several water molecules coordinate with one Mg^{2+} ion. The role of the Mg^{2+} is to activate a bound water molecule as the attacking nucleophile in the phosphodiester bond cleavage reaction. The structure of the *Giardia* Dicer confirms the intramolecular dimerization of RNase IIIa and IIIb domains and shows how the distance between the PAZ and RNase III domains matches the length of the Dicer cleavage product.

Despite much progress in understanding the molecular mechanism of the RNase III enzymes, many questions about their catalysis remain unanswered. Detailed mechanisms of the phosphodiester bond cleavage reaction are only partially understood, and the factors that stabilize the transition state and leaving group of the S_N2 (bimolecular nucleophilic substitution) reaction are not known. All but one of the published structures so far are limited to bacterial RNase III enzymes (20–24) and protozoan *Giardia* Dicer (18). These proteins are simpler than Dicers from higher eukaryotes not only in domain composition but also in the corresponding RNase III domains. In a recent study (25), a unique Argonaute-binding motif (≈127 aa) within the RNase IIIa domain of human Dicer was identified. This motif is conserved in vertebrate Dicers, but not found in nonvertebrate Dicers. Structural studies of Dicers from higher eukaryotes are needed to gain insights into the mechanisms of these proteins in dsRNA processing and subsequent events of the RNAi pathway. While this manuscript was under review, a crystal structure of the RNase IIIb domain from human Dicer was published (26). The domain forms a homodimeric structure mimicking the RNase IIIa and IIIb intramolecular interaction observed in the *Giardia* Dicer structure.

Here, we report the crystal structures of a ≈30-kDa C-terminal fragment of mouse Dicer, containing the RNase IIIb and dsRBD domains, in its apo and Cd^{2+}-bound forms at 1.68- and 2.8-Å resolution, respectively. The apo protein structure represents the highest resolution structure available to date for both RNAi-related and RNase III-related proteins. Insights from these structures, combined with results from modeling, comparative sequence analysis, and mutational/enzymatic studies, identified a lysine residue (K1790) within the RNase IIIb domain of mouse Dicer as a critical element for dsRNA cleavage. The lysine residue is highly conserved among RNase IIIa and IIIb domains of Dicer proteins, and the RNase IIIb domains of Drosha proteins, suggesting its importance in mechanisms related to dsRNA cleavage in the RNAi pathways. The possible mechanisms for the involvement of this lysine residue in the phosphodiester bond cleavage reaction and other Dicer functions are discussed.

Results and Discussion

The Crystallization Construct of Mouse Dicer Is Capable of dsRNA Cleavage. The mouse Dicer construct in our study contains the RNase IIIb and dsRBD domains. Its sequence is 98% identical to corresponding human sequence. This construct is comparable to full-length class I RNase III enzymes in terms of domain composition (Fig. 1). To test whether the construct is active in dsRNA binding and cleavage, we carried out *in vitro* dsRNA cleavage assays with a designed 52-nt stem-loop RNA containing a 24-bp stem capped by a GCAA tetraloop as the substrate. The construct is capable of Mg^{2+}-dependent dsRNA cleavage, but is not very efficient compared with *E. coli* RNase III (Fig. 2). We also note that whereas the mouse Dicer construct produces two major cleavage products (≈26 and 30 nt), the *E. coli* RNase III enzyme produces only one (≈26 nt). Studies on *A. aeolicus* RNase III enzyme (20) showed that a stem-loop RNA was cut on both strands of the stem region, producing a shorter stem-loop RNA with a 2-nt 3′ end overhang. The mouse Dicer construct and *E. coli* RNase III enzyme most likely perform similar modes of cleavage; the mouse Dicer construct might bind the stem-loop RNA in two different registration on the stem, resulting in two different cleavage products.

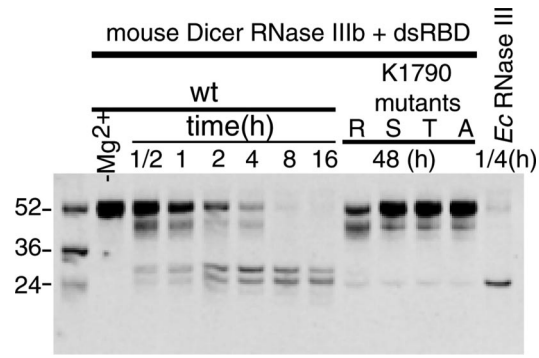

Fig. 2. *In vitro* dsRNA cleavage assays for the mouse Dicer RNaseIIIb + dsRBD protein and four point mutants (K1790 to R/S/T/A). The RNA substrate is a 52-nt stem-loop RNA with a 24-bp helical stem capped by a GCAA tetra loop. For all reactions, protein-to-RNA molar ratio is 1:1 (at 100 μM). For comparison, dsRNA cleavage by *E. coli* (Ec) RNase III is also shown (last lane).

It is known that recombinant full-length human Dicer is an inefficient enzyme *in vitro*, requiring long digestion times (12–16 h versus 1 h by *E. coli* RNase III) for complete dsRNA cleavage (www.ambion.com/techlib/tn/103/6.html). The catalytic activity of the mouse Dicer RNase IIIb + dsRBD construct is similar to that of the full-length Dicer, although its sequence and overall structure are comparable to those of bacterial RNase III enzymes (see following sections for details). Similarity between the Dicer RNase IIIb + dsRBD construct and full-length Dicer protein in dsRNA cleavage activity suggests that some determinants for cleavage inefficiency may reside in the RNase IIIb and dsRBD domains.

The Structures Reveal a Symmetric Homodimer. Structures of the apo and Cd^{2+}-bound forms of the protein were determined by single-wavelength anomalous dispersion and molecular replacement (using the apo structure as the search model), respectively [statistics for structure determination are summarized in supporting information (SI) Table 1]. Like bacterial RNase III enzymes (20–24), the mouse Dicer RNase IIIb + dsRBD construct exists as a symmetric homodimer (the dimer also exists in solution judged by gel filtration chromatography). The overall dimeric structure of the RNase IIIb domains, like the human Dicer RNase IIIb structure (26), mimics the RNase IIIa-IIIb intramolecular pseudodimer observed in the structure of *Giardia* Dicer (18). Structure of the RNase IIIb has an α-helical fold, and the dsRBD features two α-helices packed against one side of a three-stranded antiparallel β sheet. The two domains are connected by a 5-aa linker (Fig. 3*A*).

Dimerization is mediated mainly by antiparallel positioning of the α3-helices of the RNase IIIb domains, resulting in ≈1,817-Å^2 buried surface area. Hydrophobic interaction is the major driving force for dimerization. Two aromatic residues Phe-1690 and Tyr-1705, at either end of α3, participate in "ball-and-socket" interactions as the ball, inserting into a socket formed by side chains of the interacting partner (Fig. 3*B*). The ball-and-socket interaction ensures an accurate alignment of the dimerized RNaseIII domains. Notably, Phe-1690 is within the RNase III signature motif that also harbors two of the conserved catalytic carboxylates (Glu-1689 and Asp-1693).

The distance between the two active sites (each in one of the dimerized RNase III domains) is critical for the generation of 2-nt 3′ end overhang products characteristic of RNase III cleavage. Residues in the RNase IIIa domain that correspond to

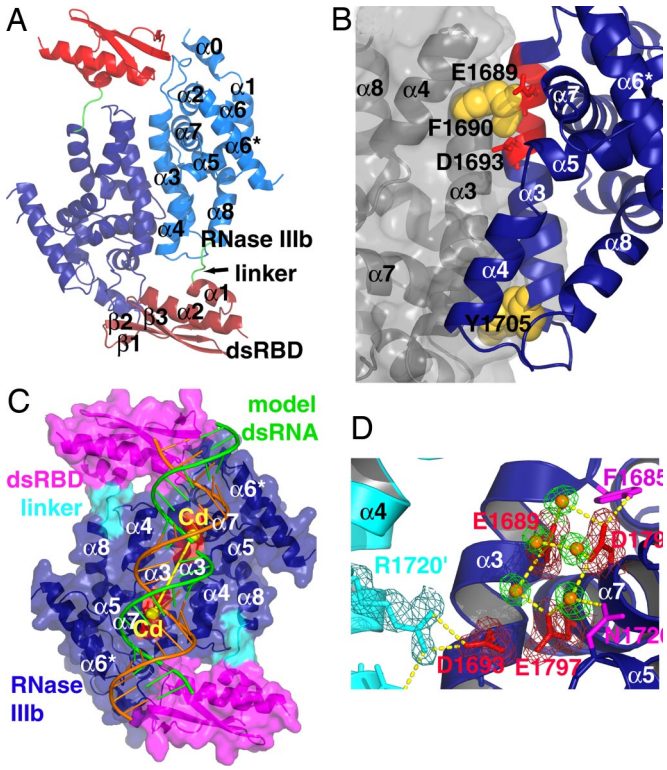

Fig. 3. Structures of mouse Dicer RNase IIIb + dsRBD. (*A*) Overall structure of the apo protein. The protein forms a symmetric homodimer. The RNase IIIb and dsRBD domains are colored in different tones of blue and red, respectively, for the different subunits. The linker is colored green. (*B*) The dimerization interface. The two RNase subunits are rendered differently with one in gray transparent surface. The two aromatic side chains involved in ball-and-socket interaction are rendered as yellow spheres. The RNase III signature motif is in red with side chains of the two conserved catalytic carboxylates shown as sticks. (*C*) Structure of the Cd^{2+}-bound structure in transparent surface. The two Cd^{2+} are shown as yellow spheres. A modeled dsRNA with broken scissile bonds is shown as ribbon. The two strands are in green and orange. The two clusters of catalytic carboxylates coordinating the Cd^{2+} ions are colored red. (*D*) Active-site structure of the apo protein. Five structured water molecules are shown as orange spheres with green density. Hydrogen bonds are represented as yellow dashed lines. Electron densities for the amino acids side chains and water molecules in the active site are contoured at 1σ of the 2 $F_o - F_c$ electron density map.

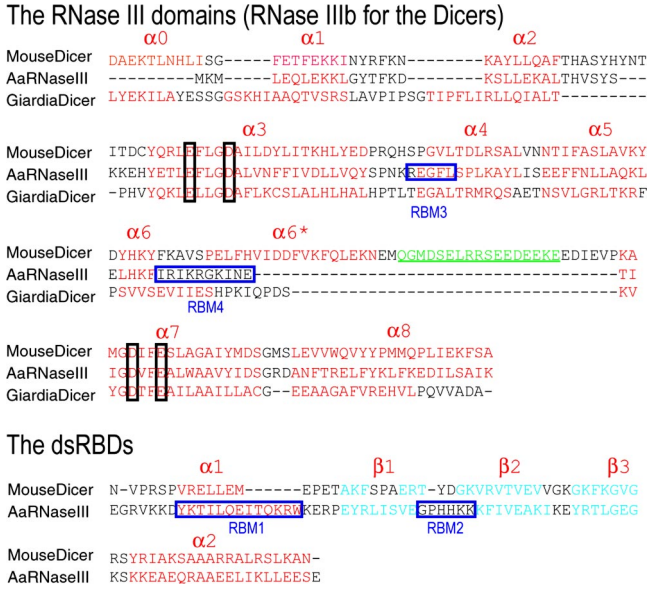

Fig. 4. Structure-based sequence alignments of the RNase IIIb and dsRBD domains of mouse Dicer with corresponding domains from *Giardia* Dicer (18) and *Aquifex* RNase III enzyme (20). The α-helices, β-strands, and loops are in red, cyan, and black, respectively. For mouse Dicer RNase IIIb domain, electron density is not observed for residues within the sequence colored in green and underlined. The four conserved carboxylates within the RNase III domains are boxed vertically. For the *Aquifex* RNase III enzyme, the four RNA-binding motifs (RBM1–RBM4) identified in the *Aquifex* RNase III enzyme–dsRNA cocrystal structure (20) are indicated by blue boxes. The α-helices and β-strands of mouse Dicer RNase IIIb and dsRBD are numbered consistent with *Aquifex* RNase III; the additional helix between α6 and α7 is therefore denoted α6*.

Phe-1690 and Tyr-1705 are Met-1307 and Phe-1322, respectively. Other residues involved in dimerization are largely conserved in the RNase IIIa domains, and the RNase IIIa and IIIb intramolecular pseudodimer of mouse Dicer should have similar dimer interface as the RNase IIIb homodimer.

The dimerization generates the catalytic valley for binding and processing dsRNAs. The two α3-helices constitute the floor of the valley. Helix α4 and the N-terminal portions of helices α5 and α7 form the ridges on either side of the valley. The molecular surface of the valley is predominantly negatively charged because of the presence of the four invariant catalytic carboxylates (Glu-1689, Asp-1693, Aps-1794, and Glu-1797) on either end of the valley (Fig. 3*C*). In the apo structure, Glu-1689/Aps-1794/Glu-1797 are involved in a hydrogen-bonding network with five water molecules and two side chains from nearby residues. Asp-1693 forms intermolecular hydrogen bonds with Arg-1720 from the partner subunit (Fig. 3*D*). In the Cd^{2+}-bound structure, each cluster of the catalytic carboxylates coordinates the binding of a Cd^{2+} ion (Fig. 3*C*). Because of the lower resolution of the structure and the bulky electron density of the Cd^{2+} ion, the accurate active site structure could not be established in the complex structure. However, intermolecular hydrogen bonds between Asp-1693 and Arg-1720 are preserved. Distance between the two Cd^{2+} ions at the two active sites is 21.5 Å. Taking into account that the metal ion is separated from the scissile phosphate by a water molecule (as the attacking nucleophile), this distance is optimal for each active site to cleave one strand of the dsRNA substrate at positions 2 bp apart from each other across the RNA helix (Fig. 3*C*).

The RNase IIIb domain, in the absence of its native interacting partner (the RNase IIIa domain from the same molecule), self-associates to form a functional homodimer. Although the homodimeric structure of the RNase IIIb domains is not native, it is catalytically active. Because each of the two active sites in the processing center is largely defined by residues from one RNase III domain, insights gained from the current structures are applicable to the genuine catalytic mechanisms of mouse Dicer.

Comparison with Previous RNase III Structures. To identify unique features of mouse Dicer, we compared the present structures to two representative previous structures of the RNase III family: *Aquifex* RNase III in complex with dsRNA cleavage products (20) and apo *Giardia* Dicer (18). Sequence of the mouse Dicer construct is comparable to the full-length *Aquifex* RNase III enzyme. Within either the RNase III or the dsRBD domain, most structural elements align quite well between the two structures (Figs. 4 and 5 *A* and *B*), although the relative orientation between the RNase III and dsRBD domains is different. Model building studies suggested that the dsRBD as determined in the apo and Cd^{2+}-bound structures would crash with dsRNA substrate (Fig. 3*C*); binding dsRNA therefore should require changes in the relative orientation between the two domains, as was seen in the *Aquifex* RNase III enzyme (20, 23).

In *Aquifex* RNase III–dsRNA complex, four RNA binding

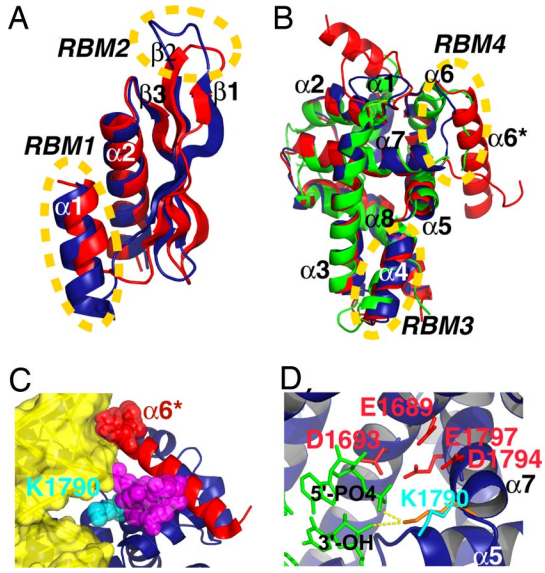

Fig. 5. Structure of mouse Dicer RNase IIIb + dsRBD in comparison with other structures and in complex with modeled dsRNA. (*A* and *B*) Comparison of mouse Dicer RNase IIIb and dsRBD domains with previous structures. (*A*) Superposition of the dsRBDs from mouse Dicer (red) and *Aquifex* RNase III enzyme (blue). (*B*) Superposition of three RNase III domains. The RNase IIIb domains from mouse and *Giardia* Dicers are colored red and green, respectively. The RNase III domain from Aa RNase III enzyme is blue. RBMs 1–4 are the four RNA binding motifs identified in the crystal structure of Aa RNase III-dsRNA complex (20). (*C* and *D*) Mouse dicer RNase IIIb domain with modeled dsRNA. (*C*) Possible bidentate interaction with both the minor and major grooves of dsRNA (surface representation in yellow) by a 45-residue region (Ser-1746–K1790) that encompass an α-helix (α6*, Ser-1746–Asn-1766, in red) and a flexible loop (density observed only for residues E1784–P1789, depicted in as magenta spheres). K1790 belongs to helix α7. Its side chain (cyan spheres) is positioned inside the major groove. (*D*) Possible roles of K1790. Side chain in cyan is the observed conformation. Slight conformational changes can position K1790 (in orange) within hydrogen bond distance to functional groups of the scissile bond (only two residues of the modeled dsRNA, in green, are shown for clarity). Side chains of the four conserved catalytic carboxylates are colored red.

motifs (RBM1–RBM4) were identified. RBM1 is the first helix, and RBM2 is the loop between strands β1 and β2 in dsRBD. Both RBM1 and RBM2 are shorter in mouse Dicer dsRBD (Figs. 4 and 5*A*). This sequence difference might correspond to weaker interaction with dsRNAs by mouse Dicer dsRBD. Moreover, in the context of the full-length native Dicer, there is only one dsRBD available for binding dsRNA. In the structure of the *Aquifex* RNase III–dsRNA product complex, dsRBD plays a dominant role in recognition and binding of dsRNA because RBM1 and RBM2 account for two-third of the RNA–protein interactions (molecular contacts). Such a dominant role is not expected for the dsRBD of mouse Dicer in native Dicer–dsRNA interaction. It is known that *in vivo* function of human Dicer requires TRBP (HIV-1 TAR RNA binding protein), which contains three dsRBDs (27, 28). It is possible that some of the dsRBDs from TRBP help Dicer in the recognition and binding of dsRNA substrates *in vivo*.

Comparisons between the two RNase IIIb domains from Dicers (mouse and *Giardia*) and the RNase III domain from *Aquifex* RNase III (Figs. 4 and 5*B*) reveal that mouse Dicer RNase IIIb shares more sequence/structure similarities with *Aquifex* RNase III domain than with the *Giardia* Dicer RNase IIIb domain. In the *Aquifex* RNase III domain, helix α4 was identified as RBM3 (20). This motif is conserved in the other two RNase III domains (Figs. 4 and 5*B*). The most outstanding difference among the three RNase III domains is found within the sequence between helices α6 and α7. In the *Aquifex* RNase III domain, a short loop connects α6 and α7. This loop was identified as the RBM4 motif in the *Aquifex* RNase III–dsRNA complex structure. In *Giardia* RNase IIIb, a short connecting loop is also found between α6 and α7, although helix α6 is longer. In mouse Dicer RNase IIIb, the sequence between helices α6 and α7 is 35–38 residues longer than those in the other two structures. This region harbors an extra helix (α6*) with five helical turns and a long loop. Density for a stretch of 17 residues within this loop was not observed, indicating high flexibility for this region (Figs. 4 and 5*B*).

A Unique Structural Motif Potentially Involved in Recognition and Processing of dsRNA. The structural features we observed within the sequence between helices α6 and α7 in the RNase IIIb domain of mouse Dicer was also present in the human Dicer RNase IIIb structure (26). The entire sequence between helices α6 and α7 is highly conserved among RNase IIIb domains of metazoan Dicers (SI Fig. 6). It may therefore represent a unique motif in RNase IIIb domains of Dicers from higher eukaryotes. To reveal possible roles of this motif, we modeled a mouse Dicer RNase IIIb–dsRNA complex based on the structure of *Aquifex* RNase III in complex with dsRNA cleavage products (20). As shown in Fig. 5*B*, most structural elements of the RNase IIIb domain from mouse Dicer align with the RNase III domain from *Aquifex* RNase III enzyme. Overlaying the common backbone atoms of the four α-helices (α3, α4, α5, and α7) that define the catalytic valley results in an rmsd of 0.56 Å. To build the complex model, we simply replaced the *Aquifex* RNase III structure with the aligned mouse Dicer RNase IIIb structure. This model has a high degree of credibility because of the high degree of similarity between the two dimeric RNase III structures. Of note, because the *Aquifex* RNase III–dsRNA structure is for a dsRNA cleavage product complex, the mouse Dicer RNase IIIb–dsRNA structural model should be closer to a product complex than to a substrate complex. In a substrate complex, the scissile bond should be positioned closer to the active-site residues of the RNase III domain (20).

The residues at the N-terminal end of helix α6* insert into the minor groove of the modeled dsRNA (Fig. 5*C*). Because of the rigidity of the helix, the residues involved in the minor groove interaction should be largely in place for the interaction before dsRNA binding. In contrast, the RBM4 loop in *Aquifex* RNase III required conformational changes to move into the minor groove of the dsRNA upon binding (20). The model also reveals possible protein–RNA interaction in the major groove, with the side chain of Lys-1790 inserting into the major groove. Therefore, the sequence between helices α6 and α7 in mouse Dicer RNase IIIb may harbor a bidentate RNA binding motif that interacts with both the minor and major grooves of dsRNAs.

A Highly Conserved Lysine Plays a Critical Role in dsRNA Cleavage. The possibility of Lys-1790 participating in dsRNA major groove interaction deserved further investigation. In the model structure, position of the Lys-1790 side chain is in close proximity to the scissile bond (Fig. 5*D*; because the model dsRNAs are cleavage products, the scissile bond is already cleaved). Starting from what is observed in the crystal structures, only slight changes in the side-chain orientation is needed to position the ε-amino group of Lys-1790 within hydrogen-bonding distance to the nonbridging phosphoryl oxygen and the O3′ leaving group of the scissile bond (in Fig. 5*D*, the potential hydrogen bonds shown as yellow dotted lines between donor and acceptor heavy atoms are 2.7 and 3.4 Å, respectively). Moreover, Lys-1790 is located at the N-terminal end of helix α7, which also harbors two of the established catalytic carboxylates Asp-1794 and Glu-1797. Lys-1790, Asp-1794, and Glu-1797 are present on the same surface of helix α7 facing the dsRNA, approximately one helical turn apart from each other. This spatial arrangement places

Lys-1790 and the cluster of catalytic carboxylates (E1689, D1693, Asp-1794, and Glu-1797) on opposite sides of the scissile bond phosphate. It is believed that a Mg^{2+} ion coordinated by the four catalytic carboxylates activates a water molecule as the attacking nucleophile in the S_N2 phosphodiester bond cleavage reaction catalyzed by RNase III enzymes (20). The interactions that stabilize the transition state and the leaving group are not known. The strategically important location of Lys-1790 makes it an excellent candidate for these jobs.

Essential involvement of a conserved catalytic lysine in phosphodiester bond cleavage reaction was documented for several phosporyl transfer enzymes, including bovine pancreatic RNase A (29–32), EcoRV endonuclease (33), human *NM23-H2* (34), *Pyrus pyrifolia* S_3-RNase (35), *Rana catesbeiana* (bullfrog) ribonuclease (36), and *E. coli* DNA topoisomerase I (37). Of particular interest are mechanisms revealed by the crystal structure of *R. catesbeiana* ribonuclease (belongs to the RNase A family) in complex with a ssRNA substrate (36). In the structure, a conserved catalytic lysine forms two hydrogen bonds with the nonbridging O_2P phosphoryl oxygen (2.60 Å) and the O3′ leaving group (3.02 Å) of the scissile bond. These interactions are strikingly similar to the model depicted in Fig. 5*D* for Lys-1790 in the mouse Dicer RNase IIIb domain.

Lys-1790 in the mouse Dicer RNase IIIb domain is conserved among the RNase IIIb domains of not only all known Dicer and Dicer-like proteins (>130 nonredundant sequence entries for many different species ranging from protozoan to human) but also all known Drosha proteins with available sequences (SI Figs. 7 and 8). This conserved lysine is also found in all but one of the RNase IIIa domains of Dicer and Dicer-like proteins (Lys-1543 in mouse Dicer RNase IIIa domain). When all available RNase IIIa and IIIb domains of Dicer and Dicer-like proteins are aligned (SI Fig. 7), Lys-1790 is one of the two highly conserved residues (the other being a glycine) close to the invariant catalytic carboxylates, suggesting possible involvement of this lysine in Dicer catalysis.

To assess the role of Lys-1790 in dsRNA cleavage, we prepared four mutants of the mouse Dicer RNase IIIb + dsRBD construct with Lys-1790 replaced by Arg/Ser/Thr/Ala, respectively. *In vitro* assays show that mutation of Lys-1790 to any one of Arg/Ser/Thr/Ala severely impaired dsRNA cleavage activity (Fig. 2; the arginine mutant seems to have somewhat higher activity than the other three mutants), indicating that Lys-1790 is really critical for dsRNA cleavage activity of the mouse Dicer RNase IIIb + dsRBD construct. Intriguingly, a serine or a threonine is found at an equivalent position in the bacterial RNase III enzyme from *E. coli* or *A. aeolicus*, respectively. Whereas the bacterial RNase III enzymes are very efficient in dsRNA cleavage, the K1790 to S/T mutations in the mouse Dicer RNase IIIb + dsRBD construct dramatically lower the activity of an already very inefficient enzyme. These results suggest that discrepancies exist between Dicers and bacterial RNase III enzymes in certain aspects of the dsRNA cleavage mechanisms. For Dicers, a highly conserved lysine in the RNase IIIa and IIIb domains may play a critical role in the phosphodiester bond cleavage reaction. By forming two hydrogen bonds to the nonbridging phosphoryl oxygen and the O3′ oxyanion leaving group of the scissile bond, the conserved lysine can stabilize the transition state and the leaving group. We showed that replacement of the lysine by an arginine, which should also have the potential to form similar hydrogen bonds, greatly reduces dsRNA cleavage activity (Fig. 2). This observation suggests that effective neutralization of the developing negative charge of the transition state may require a concentrated localized positive charge, which cannot be provided by any other amino acids but lysine (38).

We propose that the conserved lysine represents a catalytic residue in Dicers. Why would Dicers choose a catalytic lysine when other mechanisms of efficient dsRNA cleavage are available? A possible explanation is that the lysine may participate in other Dicer-specific functions besides dsRNA cleavage. It was suggested that the inefficiency of Dicer cleavage was at least partially caused by the association of Dicer with its dsRNA cleavage products (19, 39). The ability of Dicer to remain bound to its cleavage product is presumably important for Dicer to escort the miRNA/siRNA to RISC and initiate the subsequent stages of the RNAi cascade. We noted that the inefficiency in dsRNA cleavage of the mouse Dicer RNase IIIb + dsRBD construct is consistent with previous observation on recombinant full-length Dicer, suggesting that some determinants for cleavage inefficiency may reside in the RNase IIIb and dsRBD domains. It is possible that the conserved lysine remains hydrogen-bonded to the 5′ phosphate on one strand and the 3′ hydroxyl on the opposite strand of the cleavage product, thus contributes to retention of the dsRNAs.

Materials and Methods

Protein Preparation and Crystallization. The construct containing mouse Dicer RNase IIIb and dsRBD (residues 1638–1899) was cloned into pET48b vector and overexpressed as a fusion protein (with a N-terminal thioredoxin-His_6 tag removable by HRV 3C protease) in BL21(DE3) strain of *E. coli*. Expression was induced with 0.4 mM isopropyl β-D-thiogalactoside at 37°C for 3 h. Se-Met-labeled protein was prepared by using the same protocol as described (40). After lysis by sonication, the overexpressed protein was purified by Ni-NTA resin. The tag was removed by HRV 3C protease, and the cleaved sample was purified by flowing it through a Ni-NTA column. Crystals for the apo proteins were obtained by hanging-drop vapor diffusion against 20–26% PEG400, 100 mM Hepes (pH 7.0), at 22°C. To obtain the Cd^{2+}-bound crystals, crystals of the apo proteins were soaked in crystallization buffer containing 5 mM $CdCl_2$ for 24 h before data collection.

Data Collection, Structure Determination, and Refinement. Data collection was carried out at Beamlines 8.2.2 and 8.3.1 of the Advanced Light Source at Berkeley National Laboratory (Berkeley, CA). Diffraction data were integrated and reduced by using the program HKL2000 (41). The selenium atoms were located by SOLVE (42). Structure of the Cd^{2+}-bound protein was determined by molecular replacement using Phaser (43). The models was built by Coot (44) and refined with Refmac5 (45) to an *R* factor of 19.5% (R_{free} = 21.6%) for the apo structure and 26.5% (R_{free} = 32.5%) for the Cd^{2+} complex. Detailed crystallographic statistics are in SI Table 1. The figures were prepared with PyMOL (www.pymol.org).

***In Vitro* dsRNA Cleavage Assay.** A 52-nt RNA containing a 24-bp stem and a GCAA tetraloop was produced *in vitro* by using a synthetic DNA template and T7 RNA polymerase. This dsRNA was used as the substrate. The actual sequence of the RNA is available in SI Fig. 9. Two other RNAs of 36 and 24 nt, shown in Fig. 2 as size markers, were also prepared. RNA and protein were mixed and incubated at room temperature for a series of time lengths. All reactions contain 5 mM $MgCl_2$ in the reaction mixture except for the control reaction in which no Mg^{2+} was added. Cleavage reactions were analyzed by electrophoresis with 20% denaturing polyacrylamide gels. After ethidium bromide staining, the gels were visualized under UV. *E. coli* RNase III was purchased from New England BioLabs.

ACKNOWLEDGMENTS. We thank Dr. Chris Waddling for managing the University of California (San Francisco) X-Ray Crystallization Laboratory. Partial support for this work was provided by National Institutes of Health Grants AI46967 (to T.L.J.) and GM51232 (to R.M.S.).

1. Fire A, *et al.* (1998) Potent and specific genetic interference by double-stranded RNA in *Caenorhabditis elegans*. *Nature* 391:806–811.
2. Hannon GJ (2002) RNA interference. *Nature* 418:244–251.
3. Baulcombe D (2004) RNA silencing in plants. *Nature* 431:356–363.
4. Grishok A, *et al.* (2001) Genes and mechanisms related to RNA interference regulate expression of the small temporal RNAs that control *C. elegans* developmental timing. *Cell* 106:23–34.
5. Volpe TA, *et al.* (2002) Regulation of heterochromatic silencing and histone H3 Lysine-9 methylation by RNAi. *Science* 297:1833–1837.
6. Mochizuki K, Fine N, Fujisawa T, Gorovsky M (2002) Analysis of a piwi-related gene implicates small RNAs in genome rearrangement in *Tetrahymena*. *Cell* 110:689–699.
7. Elbashir SM, Lendeckel W, Tuschl T (2001) RNA interference is mediated by 21- and 22-nucleotide RNAs. *Genes Dev* 15:188–200.

8. Hutvagner G, *et al.* (2001) A cellular function for the RNA-interference enzyme Dicer in the maturation of the let-7 small temporal RNA. *Science* 293:834–838.
9. Bernstein E, Caudy AA, Hammond SM, Hannon GJ (2001) Role for a bidentate ribonuclease in the initiation step of RNA interference. *Nature* 409:363–366.
10. Hammond SM, Bernstein E, Beach D, Hannon GJ (2000) An RNA-directed nuclease mediates posttranscriptional gene silencing in *Drosophila* cells. *Nature* 404:293–296.
11. Liu Q, *et al.* (2003) R2D2, a bridge between the initiation and effector steps of the *Drosophila* RNAi pathway. *Science* 301:1921–1925.
12. Matranga C, Tomari Y, Shin C, Bartel D, Zamore P (2005) Passenger-strand cleavage facilitates assembly of siRNA into Ago2-containing RNAi enzyme complexes. *Cell* 123:607–620.
13. Rand T, Petersen S, Du F, Wang X (2005) Argonaute2 cleaves the anti-guide strand of siRNA during RISC activation. *Cell* 123:621–629.
14. Pillai RS, *et al.* (2005) Inhibition of translational initiation by Let-7 microRNA in human cells. *Science* 309:1573–1576.
15. Patel DJ, *et al.* (2006) Structural biology of RNA silencing and its functional implications. *Cold Spring Harb Symp Quant Biol* 71:81–93.
16. Parker JS, Roe SM, Barford D (2006) Molecular mechanism of target RNA transcript recognition by Argonaute-guide complexes. *Cold Spring Harb Symp Quant Biol.* 71:45–50.
17. Carmell MA, Hannon GJ (2004) RNase III enzymes and the initiation of gene silencing. *Nat Struct Mol Biol* 11:214–218.
18. Macrae IJ, *et al.* (2006) Structural basis for double-stranded RNA processing by Dicer. *Science* 311:195–198.
19. Zhang H, Kolb F, Jaskiewicz L, Westhof E, Filipowicz W (2004) Single processing center models for human Dicer and bacterial RNase III. *Cell* 118:57–68.
20. Gan J, *et al.* (2006) Structural insight into the mechanism of double-stranded RNA processing by ribonuclease III. *Cell* 124:355–366.
21. Blaszczyk J, *et al.* (2001) Crystallographic and modeling studies of RNase III suggest a mechanism for double-stranded RNA cleavage. *Structure (London)* 9:1225–1236.
22. Blaszczyk J, *et al.* (2004) Noncatalytic assembly of ribonuclease III with double-stranded RNA. *Structure (London)* 12:457–466.
23. Gan J, *et al.* (2005) Intermediate states of ribonuclease III in complex with double-stranded RNA. *Structure (London)* 13:1435–1442.
24. Akey DL, Berger JM (2005) Structure of the nuclease domain of ribonuclease III from *M. tuberculosis* at 2.1 Å. *Protein Sci* 14:2744–2750.
25. Sasakia T, Shimizu N (2007) Evolutionary conservation of a unique amino acid sequence in human DICER protein essential for binding to Argonaute family proteins. *Gene* 396:312–320.
26. Takeshita D, *et al.* (2007) Homodimeric structure and double-stranded RNA cleavage activity of the C-terminal RNase III domain of human dicer. *J Mol Biol* 374:106–120.
27. Chendrimada TP, *et al.* (2005) TRBP recruits the Dicer complex to Ago2 for microRNA processing and gene silencing. *Nature* 436:740–744.
28. Haase AD, *et al.* (2005) TRBP, a regulator of cellular PKR, HIV-1 virus expression, interacts with Dicer and functions in RNA silencing. *EMBO Rep* 6:961–967.
29. Nogués M, Vilanova M, Cuchillo C (1995) Bovine pancreatic ribonuclease A as a model of an enzyme with multiple substrate binding sites. *Biochim Biophys Acta* 1253:16–24.
30. McPherson A, Brayer G, Cascio D, Williams R (1986) The mechanism of binding of a polynucleotide chain to pancreatic ribonuclease. *Science* 232:765–768.
31. Fontecilla-Camps JC, de Llorens R, le Du MH, Cuchillo CM (1994) Crystal structure of ribonuclease A.d(ApTpApApG) complex: Direct evidence for extended substrate recognition. *J Biol Chem* 269:21526–21531.
32. Raines RT (1998) Ribonuclease A. *Chem Rev* 98:1045–1066.
33. Horton NC, Newberry KJ, Perona JJ (1998) Metal ion-mediated substrate-assisted catalysis in type II restriction endonucleases. *Proc Natl Acad Sci USA* 95:13489–13494.
34. Postel EH, Abramczyk BM, Levit MN, Kyin S (2000) Catalysis of DNA cleavage and nucleoside triphosphate synthesis by NM23–H2/NDP kinase share an active site that implies a DNA repair function. *Proc Natl Acad Sci USA* 97:14194–14199.
35. Matsuura T, *et al.* (2001) Crystal structure at 1.5-Å resolution of *Pyrus pyrifolia* pistil ribonuclease responsible for gametophytic self-incompatibility. *J Biol Chem* 276:45261–45269.
36. Leu Y-J, *et al.* (2003) Residues involved in the catalysis, base specificity, and cytotoxicity of ribonuclease from *Rana catesbeiana* based upon mutagenesis and x-ray crystallography. *J Biol Chem* 278:7300–7309.
37. Strahs D, Zhu C-X, Cheng B, Chen J, Tse-Dinh Y-C (2006) Experimental and computational investigations of Ser10 and Lys13 in the binding and cleavage of DNA substrates by *Escherichia coli* DNA topoisomerase I. *Nucleic Acids Res* 34:1785–1797.
38. Bash P, Singh U, Langridge R, Kollman P (1987) Free energy calculations by computer simulation. *Science* 236:564–568.
39. Zhang H, Kolb FA, Brondani V, Billy E, Filipowicz W (2002) Human Dicer preferentially cleaves dsRNAs at their termini without a requirement for ATP. *EMBO J* 21:5875–5885.
40. Du Z, *et al.* (2005) Crystal structure of the first KH domain of human poly(C)-binding protein-2 in complex with a C-rich strand of human telomeric DNA at 1.7 Å. *J Biol Chem* 280:38823–38830.
41. Otwinowski W (1997) Processing of x-ray diffraction data collected in oscillation mode. *Methods Enzymol* 276:307–326.
42. Terwilliger TC, Berendzen J (1999) Automated MAD, MIR structure solution. *Acta Crystallogr D* 55:849–861.
43. McCoy AJ, Grosse-Kunstleve RW, Storoni LC, Read RJ (2005) Likelihood-enhanced fast translation functions. *Acta Crystallogr D* 61:458–464.
44. Emsley P, Cowtan K (2004) Coot: Model-building tools for molecular graphics. *Acta Crystallogr D* 60:2126–2132.
45. Murshudov GN, Vagin AA, Dodson EJ (1997) Refinement of macromolecular structures by the maximum-likelihood method. *Acta Crystallogr D* 53:240–255.